HHS Public Access

Author manuscript

Nat Neurosci. Author manuscript; available in PMC 2018 April 17.

Published in final edited form as:

Nat Neurosci. 2017 November ; 20(11): 1540–1548. doi:10.1038/nn.4649.

Synapse-specific astrocyte gating of amygdala-related behavior

Mario Martin-Fernandez[1], **Stephanie Jamison**[1], **Laurie M Robin**[2,3], **Zhe Zhao**[2,3], **Eduardo D Martin**[4], **Juan Aguilar**[5,iD], **Michael A Benneyworth**[6], **Giovanni Marsicano**[2,3], and **Alfonso Araque**[1,iD]

[1]Department of Neuroscience, University of Minnesota, Minneapolis, Minnesota, USA

[2]INSERM, U1215 NeuroCentre Magendie, Endocannabinoids and Neuroadaptation, Bordeaux, France

[3]Université de Bordeaux, Bordeaux, France

[4]Instituto Cajal, Consejo Superior de Investigaciones Científicas. Madrid, Spain

[5]Hospital Nacional de Parapléjicos, Servicio de Salud de Castilla–La Mancha, Toledo, Spain

[6]Mouse Behavior Core, University of Minnesota, Minneapolis, Minnesota, USA

Abstract

The amygdala plays key roles in fear and anxiety. Studies of the amygdala have largely focused on neuronal function and connectivity. Astrocytes functionally interact with neurons, but their role in the amygdala remains largely unknown. We show that astrocytes in the medial subdivision of the central amygdala (CeM) determine the synaptic and behavioral outputs of amygdala circuits. To investigate the role of astrocytes in amygdala-related behavior and identify the underlying synaptic mechanisms, we used exogenous or endogenous signaling to selectively activate CeM astrocytes. Astrocytes depressed excitatory synapses from basolateral amygdala via A_1 adenosine receptor activation and enhanced inhibitory synapses from the lateral subdivision of the central amygdala via A_{2A} receptor activation. Furthermore, astrocytic activation decreased the firing rate of CeM neurons and reduced fear expression in a fear-conditioning paradigm. Therefore, we conclude that astrocyte activity determines fear responses by selectively regulating specific synapses, which indicates that animal behavior results from the coordinated activity of neurons and astrocytes.

Correspondence should be addressed to A.A. (araque@umn.edu).
Juan Aguilar http://orcid.org/0000-0002-8070-3923
Alfonso Araque http://orcid.org/0000-0003-3840-1144

Note: Any Supplementary Information and Source Data files are available in the online version of the paper.

AUTHOR CONTRIBUTIONS

M.M.-F. and A.A. conceived the study. M.M.-F., J.A., G.M. and A.A. wrote the manuscript. M.M.-F. performed and analyzed electrophysiological and calcium imaging experiments and analyzed the data. M.M.-F., E.D.M., J.A. and A.A. designed *in vivo* electrophysiological experiments. S.J. performed immunohistochemistry techniques. M.M.-F., M.A.B., G.M. and A.A. designed the behavioral experiments. M.A.B., L.M.R. and Z.Z. performed behavioral experiments. All the authors read and edited the manuscript.

COMPETING FINANCIAL INTERESTS

The authors declare no competing financial interests.

The amygdala, which encompasses several anatomical and functional subnuclei, plays critical roles in a variety of behavioral responses, including fear and anxiety[1]. It is constituted primarily by the basolateral amygdala (BLA) and central amygdala (CeA)[1–3]. The BLA contains a majority of spiny glutamatergic neurons[4] and is the main input structure of the amygdala, receiving multimodal sensory information from thalamus[5] and cortex[6]. The CeA contains a majority of GABAergic projecting neurons[7] and can be divided into lateral (CeL) and medial (CeM) nuclei[1–3, 7]. The CeM, which receives excitatory and inhibitory inputs from the BLA and CeL, respectively, is the major output subnucleus projecting to the brainstem and hypothalamus to control autonomic and motor responses[2, 3, 8, 9]. Recently, great progress has been made in elucidating the role of the CeA and its neuronal populations in processing emotionally relevant information[10–16], but the role of glial cells in the CeA remains largely unknown. Elucidating the role of astrocytes in the amygdala may provide a deeper understanding of information processing that occurs in this area.

While they are already recognized for their classical metabolic, protective and supportive roles, astrocytes are now emerging as key determinants of synaptic function[17–20]. They express receptors that are activated by neurotransmitters[21–23] and release gliotransmitters that activate neuronal receptors[17, 24]. Through the release of gliotransmitters, astrocytes are able to regulate synaptic transmission[17, 22, 25–27] and affect animal behavior[28–31]. Important progress has been made toward defining the mechanisms of synaptic regulation by astrocytes[17, 20], and behavioral effects have been observed after the disturbance of astrocytic molecular events[28–31]. Yet it remains unknown how physiological astrocyte activity regulates the synaptic and circuit functions that underlie specific behaviors. In the present study we aimed to fill the mechanistic gap between astrocyte-dependent regulation of synaptic function and behavior. The amygdala is an ideal structure for such an investigation because it is involved in well-characterized behaviors such as the expression of conditioned fear responses with a clear readout. Using endocannabinoids (eCBs) and designer receptors exclusively activated by designer drugs (DREADDs) as, respectively, endogenous and exogenous stimuli to activate astrocytes, we found that astrocytes regulated neurotransmission in specific synapses of the CeM through differential mechanisms. Astrocytes depressed excitatory synapses from the BLA via A_1 receptor activation, whereas they enhanced inhibitory synapses from the CeL via A_{2A} receptor activation. Consistent with these results, astrocytes decreased the CeM neuronal firing rate and influenced fear expression.

RESULTS

CeM astrocytes respond to endogenously mobilized endocannabinoids

To investigate the effects of astrocyte activation on synaptic transmission in the CeM, we recorded excitatory postsynaptic currents (EPSCs) and inhibitory postsynaptic currents (IPSCs) evoked by the stimulation of BLA and CeL, respectively (Supplementary Fig. 1a,b), and stimulated astrocytes with either eCBs released by neurons, as an endogenous stimulus, or chemogenetic activation of Gqprotein-coupled DREADDs expressed in astrocytes, as a specific stimulus. First, we tested whether CeM astrocytes respond to eCBs[32–34] released by CeM neurons during neuronal depolarization (ND; 0 mV, 10 s)[35, 36] by monitoring calcium

levels in astrocytes (Fig. 1a), identified with SR101 (Supplementary Fig. 1c). ND increased the level of astrocytic calcium (Fig. 1b) and increased the calcium event probability (138 astrocytes from $n = 10$ slices; $P < 0.001$; Fig. 1c,d). This effect was abolished by the CB1R antagonist AM251 (2 μM; 127 astrocytes from $n = 7$ slices; $P = 0.96$); in addition, it was absent in GFAP-CB1R–null mice (175 astrocytes from $n = 10$ slices; $P = 0.63$), which lack CB1 receptors specifically in astrocytes[30]; present in wild-type littermates that expressed CB1 receptors (GFAP-CB1^{WT}; 97 astrocytes from $n = 9$ slices; $P = 0.006$); and absent in IP3R2-null mice, in which G-protein-mediated calcium elevation is selectively impaired in astrocytes[33, 37] (74 astrocytes from $n = 8$ slices; $P = 0.73$; Fig. 1d). Furthermore, our analysis of the ND-evoked calcium event probability in different conditions indicated that the observed increase in control was abolished in the presence of AM251 and in GFAP-CB1R–null and IP3R2-null mice (two-way analysis of variance (ANOVA) indicated a significant effect of ND ($P < 0.001$) and an interaction with the 'experimental condition' ($P < 0.001$); Supplementary Table 1; *post hoc* Holm–Sidak, $P = 0.004$, $P = 0.003$ and $P < 0.001$, respectively). In contrast, we did not observe any statistical differences when we compared the control condition with the GFAP-CB1^{WT} mice ($P = 0.421$; Fig. 1d). Taken together, these results indicate that eCBs released from CeM neurons activate astrocytic CB1Rs that increase calcium levels in astrocytes.

CB1R–dependent activation of astrocytes potentiates CeL–CeM inhibitory synaptic transmission

We then investigated whether astrocytes regulate synaptic transmission in CeM neurons. We obtained paired recordings[33, 38] of CeM neurons, depolarized one neuron (homoneuron) to induce the release of eCBs (which elevated astrocytic calcium), and recorded either CeL-evoked IPSCs or BLA-evoked EPSCs in the paired neuron (heteroneuron) to exclude direct presynaptic effects of eCBs[35] (Fig. 1e,i). We pharmacologically isolated IPSCs and EPSCs (Supplementary Fig. 1b) and adjusted the stimulus parameters to stimulate single or a few presynaptic fibers[26, 27, 38, 39] that induced failures or successes in synaptic responses. We quantified the probability of release (Pr; i.e., the proportion of successful responses) and the synaptic potency (i.e., the amplitude of the successful responses). ND induced a transient increase in the CeL-evoked IPSC Pr ($n = 22$; $P < 0.001$) recorded in the heteroneuron (Fig. 1f,g), with no changes in the synaptic potency ($n = 22$; $P = 0.88$; Supplementary Fig. 2a,b), suggesting a presynaptic mechanism. Consistent with this idea, the increase in the Pr was associated with a decrease in the paired pulse ratio (PPR; from 1.1 ± 0.02 to 1.04 ± 0.2 (mean ± s.e.m.); $n = 17$; $P = 0.007$, paired *t*-test). The ND-induced increase in the CeL-evoked IPSC Pr was abolished by AM251 ($n = 11$; $P = 0.74$) and was absent in GFAP-CB1R–null mice ($n = 7$; $P = 0.21$) and IP3R2^{-} mice ($n = 10$; $P = 0.3$; Fig. 1h) but present in GFAP-CB1^{WT} littermates ($n = 7$; $P = 0.008$), indicating that the ND-evoked synaptic regulation was mediated by the activation of astrocytic CB1Rs and calcium mobilization. Astrocytic CB1R activation by eCBs stimulates the release of astrocytic glutamate in other brain regions, such as hippocampus, cortex and striatum[33, 34, 38]. However, the ND-induced increase in the CeL-evoked Pr of IPSCs was unaffected by treatment with antagonists of group I metabotropic glutamate receptors (mGluRs) MPEP (50 μM) and LY367385 (100 μM; $n = 10$; $P = 0.0038$; Fig. 1h). Elevated calcium levels in astrocytes have been shown to trigger the release of ATP, which, after being converted to adenosine, may regulate synaptic

transmission[17, 27]. The increase in the CeL-evoked IPSC Pr was abolished by the antagonist of adenosine A_{2A} receptors SCH 58261 (100 nM; $n = 7$; $P = 0.22$), but not by the antagonist of adenosine A_1 receptors CPT (5 μM; $n = 13$; $P = 0.006$; Fig. 1h). Furthermore, the analysis of the Pr after ND indicated that ND-evoked Pr changes were prevented in the presence of AM251 and SCH, and in GFAP-CB1R–null and IP3R2-null mice (two-way ANOVA indicated a significant effect of ND ($P < 0.001$) and an interaction with the experimental condition ($P < 0.001$); Supplementary Table 1; *post hoc* Holm–Sidak, $P < 0.001$ for the four conditions), but were unaffected in the presence of antagonists of mGluRs (MPEP + LY) and A_1 receptors (CPT) and in GFAP-$CB1^{WT}$ mice ($P = 0.35$, $P = 0.45$ and $P = 0.18$, respectively; Fig. 1h). To test whether Pr changes depend on the basal synaptic Pr, we compared the absolute basal Pr values in the different experimental conditions. We did not observe any significant differences between the basal Pr values of the different experimental conditions (one-way ANOVA, $P = 0.07$; Supplementary Fig. 3a). Furthermore, we obtained similar results when we analyzed either absolute or normalized Pr values in the different conditions (Supplementary Table 2a).

Together, these results suggest that ND-induced astrocyte activation stimulates the release of ATP/adenosine that acts on neuronal receptors to regulate inhibitory synaptic transmission. To test the idea that the adenosine-receptor activation occurs downstream from the astrocytic calcium activity, we analyzed the effects of A_{2A} and A_1 receptor antagonists on the ND-evoked astrocyte calcium signal. We observed that ND evoked an increase in the calcium event probability in the presence of SCH (from 0.25 ± 0.3 to 0.46 ± 0.6; 96 astrocytes from $n = 6$ slices; paired *t*-test, $P = 0.01$) and CPT (from 0.21 ± 0.1 to 0.47 ± 0.4; 115 astrocytes from $n = 7$ slices; paired *t*-test, $P = 0.01$).

Taken together, these results indicate that eCBs mobilized by CeM neurons increase calcium levels in astrocytes through the activation of CB1Rs, which leads to the activation of A_{2A} receptors, thus increasing the CeL-evoked IPSC Pr.

Astrocytic CB1R–dependent regulation of BLA–CeM excitatory synaptic transmission

We next investigated the effects of eCB signaling on the Pr of BLA-evoked EPSCs in CeM neurons. In a paired-neuronal-recording approach, we recorded BLA-evoked EPSCs in the heteroneuron (Fig. 1i). In contrast to the effects on IPSCs, ND evoked a transient decrease in the EPSC Pr ($n = 24$ neurons; $P = 0.004$; Fig. 1j,k) without modifying the synaptic potency ($n = 24$ neurons; $P = 0.2$; Supplementary Fig. 2c,d). The PPR increased from 0.98 ± 0.03 to 1.12 ± 0.04 ($n = 12$; $P = 0.001$, paired *t*-test), suggesting a presynaptic mechanism. The ND-evoked depression of EPSCs was abolished by AM251 ($n = 12$; $P = 0.66$) and absent in GFAP-CB1R–null ($n = 11$; $P = 0.25$) and IP3R2-null mice ($n = 10$; $P = 0.17$), but present in the presence of mGluR antagonists MPEP and LY367385 (100 μM; $n = 13$; $P = 0.01$; Fig. 1l) and in GFAP-$CB1^{WT}$ littermates ($n = 9$; $P = 0.003$; Fig. 1l). Moreover, the decrease in EPSC Pr was abolished by the A_1 adenosine-receptor antagonist CPT ($n = 9$; $P = 0.14$), but not by the A_{2A}-receptor antagonist SCH 58261 ($n = 12$; $P = 0.04$; Fig. 1l). CPT is known to enhance basal synaptic transmission in some brain regions, such as the hippocampal CA1 area, which is tonically inhibited by presynaptic adenosine receptors[40, 41]. However, this does not seem to be the case in the CeM, as similar Pr values were found in the absence and

presence of CPT (EPSC Pr control, 0.47 ± 0.04 (n = 24); CPT, 0.37 ± 0.07 (n = 9); unpaired t-test, P < 0.24; IPSC Pr, 0.39 ± 0.04 and 0.47 ± 0.02; unpaired t-test, P = 0.21). Furthermore, although we cannot totally exclude the possibility that BLA stimulation affects synaptic transmission in the CeM indirectly through the CeL, this is unlikely, because BLA-evoked EPSCs were assessed in the presence of GABA-receptor antagonists.

Taken together, these results suggest that eCBs mobilized by ND increase of astrocyte calcium levels through the activation of CB1 receptors, thus resulting in the activation of A_1 presynaptic receptors and decreasing the BLA-evoked EPSC Pr (Fig. 1l). Furthermore, the combined statistical analysis indicated that the ND-evoked response observed in the control condition was absent in the presence of AM251 and CPT and in GFAP-CB1R- and IP3R2-null mice (two-way ANOVA indicated a significant effect of ND (P < 0.001) and an interaction with the experimental condition (P < 0.001); Supplementary Table 1; *post hoc* Holm–Sidak, P < 0.001; P < 0.001, P < 0.001 and P = 0.002, respectively). We did not note any differences relative to the control in the presence of MPEP + LY and SCH or in GFAP-$CB1^{WT}$ mice (P = 0.46, P = 0.96 and P = 0.98, respectively; Fig. 1l). In addition, we did not observe any statistical differences when we compared the absolute basal Pr values in the different experimental conditions (one-way ANOVA, P = 0.073; Supplementary Fig. 3b), which suggests that the effects of ND were independent of the basal Pr. Furthermore, we obtained similar statistical results when we compared either absolute or basal-normalized Pr values in different conditions (Supplementary Table 2b). Notably, we found similar basal Pr values in GFAP-$CB1R^{WT}$ and GFAP-CB1R–null mice (EPSC Pr, 0.5 ± 0.07 (n = 11) and 0.39 ± 0.07 (n = 9), respectively; unpaired t-test, P = 0.28; IPSC Pr, 0.55 ± 0.07 (n = 7) and 0.47 ± 0.06 (n = 10), respectively; unpaired t-test, P = 0.4), suggesting that eCBs do not tonically activate astrocytes, which are instead acutely activated by eCBs released on demand under neuronal stimulation.

Besides glutamate and ATP/adenosine, D-serine is another major gliotransmitter known to regulate synaptic transmission in other brain areas by acting as co-agonist of NMDA receptors (NMDARs)[25, 42]. A contribution of D-serine to the astrocyte-mediated regulation of inhibition here is unlikely because we isolated CeL-evoked IPSCs by recording in the presence of the NMDAR antagonist D-AP5. To investigate the involvement of D-serine in the regulation of BLA-evoked EPSCs, we tested the ND-evoked effects in the presence of D-AP5, which did not prevent the ND-dependent decrease of BLA-evoked EPSC Pr (96.9 ± 2.2 and 75.6 ± 5.5 before and after ND, respectively; n = 10; paired t-test, P = 0.003). Therefore, although different synaptic regulatory mechanisms may be mediated by D-serine, the present results suggest that it is not involved in this phenomenon. Taken together, the present results indicate that eCBs differentially regulate inhibitory and excitatory synaptic transmission by stimulating astro-cytes, which in turn leads to the activation of A_{2A} and A_1 adenosine receptors (Fig. 1h,l).

We then investigated whether these phenomena were present in the same CeM neuron (Supplementary Fig. 4a). First, we pharmacologically isolated CeL-evoked IPSCs and monitored the ND-evoked increase in IPSC Pr (n = 6; P = 0.02; Supplementary Fig. 4b,c); then we relocated the stimulation pipette in the BLA and, after washing out inhibitors of excitatory transmission, pharmacologically isolated EPSCs (Supplementary Fig. 4a,b). In

these conditions, ND induced a decrease in EPSC Pr values recorded in the same neuron (n = 6; P = 0.04; Supplementary Fig. 4b,c), indicating that astrocyte activation by eCBs in the CeM differentially regulates excitatory and inhibitory synapses in the same neurons, affecting the excitatory/inhibitory balance of CeM neurons.

Increased astrocyte calcium is necessary for CB1R-dependent synaptic regulation

The results presented above show that both eCB-mediated excitatory and inhibitory synaptic regulation were absent in mice that lacked IP3R2 (Fig. 1h,l), which largely mediates G-protein-mediated calcium elevation in astrocytes, thus suggesting that synaptic regulation requires the elevation of calcium levels in astrocytes. Because other types of IP_3 receptors have recently been shown to contribute to astrocyte calcium mobilization[43], we further tested the astrocytic calcium dependency by loading astrocytes with the calcium chelator BAPTA, by whole-cell patch-clamping astrocytes with a solution containing 40 mM BAPTA. Astrocytes are known to be gap-junction coupled in different brain areas, which allows the diffusion of BAPTA in the astrocytic network from single recorded astrocytes[44, 45]. We confirmed that astrocytes in the CeM are also gap-junction coupled, as biocytin included in a single patch-clamped astrocyte diffused to neighboring astrocytes (Fig. 2a). Then, we either filled astrocytes with BAPTA or placed a BAPTA-containing pipette in the extracellular space as the control, to rule out potential effects of BAPTA leakage in the extracellular space (Fig. 2b). Although ND increased the astrocyte calcium event probability in the control conditions (i.e., when the BAPTA-containing pipette was located extracellularly (117 astrocytes from n = 7 slices; P < 0.001; Fig. 2b,c)), we did not observe any calcium changes in response to ND in astrocytes filled with BAPTA (131 astrocytes from n = 9 slices; P = 0.16; Fig. 2b,c), which indicated that loading astrocytes with BAPTA prevented ND-evoked astrocytic calcium responses.

We then tested the effects of astrocyte BAPTA-loading on CeL-evoked IPSCs and BLA-evoked EPSCS. In this condition, ND did not affect the CeL-evoked IPSC Pr (n = 8; P = 0.16; Fig. 2d,e) or the BLA-evoked EPSC Pr (n = 8; P = 0.6; Fig. 2f,g), whereas an increase in the CeL-evoked IPSC Pr (n = 9; P = 0.003; Fig. 2e) and a decrease in the BLA-evoked EPSC Pr (n = 11; P = 0.03; Fig. 2g) were observed in the control condition. Taken together, these results indicate that the observed synaptic regulation requires astrocyte calcium elevations (Fig. 2).

Chemogenetic astrocyte activation regulates CeM synaptic transmission

If synaptic regulation by astrocytic calcium elevations is a general phenomenon, astrocyte stimulation should be able to produce similar effects independent of eCB actions. To test this idea, we used an artificial but cell-specific stimulus to directly activate astrocytes. We injected mCherry-tagged adeno-associated virus (AAV8-GFAP-hM3D(Gq)–mCherry) into the CeM of mice to induce selective expression of the stimulatory Gq-DREADD hM3D in astrocytes (Fig. 3a,b; detailed information is provided in the Online Methods). Local application of the selective ligand clozapine-N-oxide (CNO; 1 mM) by pressure pulse (2 s) increased calcium levels and the calcium event probability in DREADD-expressing astrocytes (78 astrocytes from n = 7 slices; P = 0.0018; Fig. 3c,d). To confirm that these effects were selectively mediated by CNO activation of DREADDs, we locally applied

either extracellular solution without CNO to DREADD-expressing astrocytes (105 astrocytes from $n = 8$ slices) or CNO in mice that lacked DREADD expression (109 astrocytes from $n = 8$ slices). In both cases, we observed no increases in calcium event probability ($P = 0.17$ and $P = 0.83$, respectively; Fig. 3d). In agreement with the effects produced by eCB-mediated astrocyte activation (Fig. 1h,l), selective stimulation of DREADD-expressing astrocytes by CNO increased the Pr of CeL-evoked IPSCs ($n = 7$; $P = 0.004$) and decreased the Pr of BLA-evoked EPSCs ($n = 8$; $P = 0.02$; Fig. 3e–h), with no changes in synaptic potencies (IPSCs, $n = 7$, $P = 0.83$; EPSCs, $n = 8$, $P = 0.2$; Supplementary Fig. 5). Furthermore, the CNO-evoked increase in IPSC Pr was blocked by the A_{2A} receptor antagonist SCH58261 ($n = 7$; $P = 0.96$; Fig. 3f), and the CNO-evoked decrease in EPSC Pr was blocked by the A_1 receptor antagonist CPT ($n = 7$; $P = 0.3$; Fig. 3h). Therefore, direct activation of DREADD-expressing astrocytes produced similar synaptic effects as eCB-mediated activation of astrocytes by increasing astrocyte calcium levels and stimulating gliotransmitter release. To further test this idea, which suggested that the chemogenetic activation is independent of astrocytic CB1R activation, we applied CNO locally in the presence of the CB1R antagonist AM 251. In this condition, CNO increased the calcium event probability (from 0.21 ± 0.02 to 0.74 ± 0.1; 69 astro-cytes from $n = 6$ slices; $P = 0.004$, paired t-test), increased the Pr of CeL-evoked IPSCs ($n = 8$; $P = 0.003$) and decreased the Pr of BLA-evoked EPSCs ($n = 6$; $P = 0.02$; Fig. 3f,h), with no changes observed in synaptic potencies (IPSCs, $n = 8$, $P = 0.87$; EPSCs, $n = 6$, $P = 0.77$; Supplementary Fig. 5a,b). These results indicate that selective activation of DREADD-expressing astrocytes mimics the effects of eCBs as endogenous stimuli: both induced elevations in astrocyte calcium levels that led to an increase in IPSC Pr and a decrease in EPSC Pr. Thus, astrocyte stimulation by the activation of endogenous receptors (CB1Rs stimulated by eCBs mobilized from neurons) or exogenous but selective receptors (Gq-DREADDs activated by CNO) differentially regulate inhibitory and excitatory synapses in CeM neurons.

Next, we investigated the effects of sustained application of CNO (10 μM). Perfusion of the agonist induced a persistent increase in the calcium oscillation frequency ($n = 74$ astrocytes, $n = 6$ slices; $P = 0.009$; Supplementary Fig. 6a,b), a tonic increase in the Pr of CeL-evoked IPSCs ($n = 9$; $P = 0.001$; Supplementary Fig. 6c,d), and a tonic decrease in the Pr of BLA-evoked EPSCs ($n = 6$; $P = 0.0001$; Supplementary Fig. 6e,f). Consistent with observations after the acute application of CNO, the effects on IPSCs and EPSCs were not accompanied by changes in the synaptic potency (IPSCs, $n = 9$, $P = 0.27$; EPSCs, $n = 6$, $P = 0.59$; Supplementary Fig. 5c,d) and were reversed by the A_{2A} receptor antagonist SCH58261 ($n = 3$; $P = 0.88$; Supplementary Fig. 6c,d) and by the A_1 receptor antagonist CPT ($n = 4$; $P = 0.23$; Supplementary Fig. 6e,f), respectively. Taken together, these results suggest that persistent application of CNO induces a tonic activation of astrocytes and a tonic regulation of both BLA–CeM excitatory and CeL–CeM inhibitory synaptic inputs.

In vivo functional consequences of astrocytic activation

We then asked whether the astrocytic differential synaptic regulation observed in acute brain slices would alter the firing rate of CeM neurons *in vivo*. For this purpose, we injected DREADDs into CeM, which allowed us to locally activate a population of astrocytes (Fig.

4a) during *in vivo* electrophysiological recording of a neural population within the same CeM in anesthetized animals. We obtained basal electrophysiological recordings of multi-unit activity under control conditions (over 30 min) and after an intraperitoneal (i.p.) injection of CNO (2 mg/kg body weight). In mice expressing Gq-DREADDs in CeM astrocytes after injection with AAV8-GFAP-hM3D(Gq)– mCherry, CNO decreased the CeM firing rate ($n = 28$ neurons from 7 mice; $P = 0.004$; Fig. 4b,c), whereas no changes were observed after saline injection ($n = 23$ neurons from 6 mice; $P = 0.6$; Fig. 4c). This relative silencing of CeM neural activity is consistent with the increased inhibitory synaptic rate and decreased rate of excitatory synaptic inputs (Fig. 3f,h).

Finally, we studied the consequences of selective activation of CeM astrocytes on amygdala-related behavior by using the delayed auditory fear conditioning paradigm (Fig. 4a,d). Three weeks after receiving virus injections to induce DREADD expression in CeM astrocytes, mice underwent cued fear conditioning. On test day 1, 24 h after training, mice received i.p. injections of either CNO ($n = 33$) or saline ($n = 30$) 30 min before presentation of the first non-reinforced cue, at which point the freezing response was recorded (Fig. 4d). In these conditions, saline-injected mice did not show any reduction of freezing during the 3 min of cue presentation (i.e., no within-session extinction), whereas in test 1, animals injected with CNO showed a clear extinction of the freezing response and a decreased fear response to the cue compared with saline-injected animals ($P = 0.037$, $P < 0.001$, $P < 0.001$; Fig. 4e). Notably, 24 h after CNO or saline injection, on test day 2, no differences were observed between the freezing responses of the two animal cohorts ($P = 0.23$, $P = 0.24$, $P = 0.066$; Fig. 4e), indicating that CNO produced an acute effect in test 1 that was not present 24 h after the CNO application, in test 2. We also tested the effects of astrocytic activation in the elevated plus maze, a behavioral paradigm associated with anxiety behavior. We did not observe any differences in the percentage of time spent in the open arms of the maze ($P = 0.44$; Fig. 4f). Furthermore, CNO did not produce any behavioral effects in mice that lacked DREADD expression (Supplementary Fig. 7). These results indicate that selective activation of astrocytes in the CeM specifically enhances within-session extinction and reduces the expression of an acquired fear response, without altering long-term extinction of the same behavior or anxiety-like behavior. Rather than acting in a broad, unspecific manner, astrocytes influence certain specific behaviors, which is consistent with specific synaptic regulation.

DISCUSSION

A growing body of evidence suggests that astrocyte–neuron interactions are crucial elements in the control of synaptic physiology[26, 27] and neuronal networks[33, 46]. Our results show that astrocytes differentially regulate both excitatory and inhibitory synaptic transmission in the CeM in a synapse-specific manner, thus resulting in the regulation of neuronal activity and influencing the behavioral output of the brain region (Supplementary Fig. 8).

The present results indicate that astrocytes in the central amygdala are functional components of the eCB system. In agreement with reports of other brain areas, eCBs regulate synaptic transmission through the activation of CB1Rs in astrocytes, calcium mobilization and the stimulation of gliotransmitter release[32, 34, 38, 47]. In addition to the

well-known regulation of synaptic transmission and plasticity by eCBs through direct activation of neuronal CB1Rs[48, 49] (Supplementary Fig. 9), the present results add to the accumulating evidence indicating that eCBs may have additional synaptic regulatory effects by activating astrocytes, which can expand the signal range and regulate synapses relatively distant from the eCB source, a phenomenon termed lateral regulation of synaptic transmission[50]. These complementary mechanisms of neuron- and astrocyte-driven signaling provide a high degree of complexity to the functional consequences of eCB signaling.

Astrocytes are able to release different neuroactive substances. Among them, glutamate ATP/adenosine and D-serine are the major gliotransmitters identified as regulators of synaptic transmission in several brain areas[17]. Our results indicate that the synaptic regulation observed in our experimental conditions depends on astrocyte calcium activity that stimulates the release of ATP/adenosine, which, acting as a gliotransmitter, activates neuronal adenosine receptors in CeM synapses. The astrocyte-mediated synaptic regulation of both CeL-evoked IPSCs and BLA-evoked EPSCs was insensitive to mGluR antagonists, which suggests that the gliotransmitter glutamate is not involved. Similarly, the insensitivity of the synaptic regulation to D-AP5 suggests that D-serine, which acts as a co-agonist of NMDARs[25, 42], is not implicated. Therefore, although these gliotransmitters might have other potential effects, their involvement in the reported phenomena is unlikely. In contrast, our results show that synaptic regulation of CeL-evoked IPSCs and BLA-evoked EPSCs was prevented by A_{2A} and A_1 receptor antagonists, respectively, suggesting that ATP/adenosine is the gliotransmitter responsible for the phenomena (Supplementary Fig. 8).

The selective signaling of astrocytes to specific synapses belonging to specific pathways has been reported recently in basal ganglia circuits[33]. The synapse specificity of astrocytic signaling is further supported by the present results, which show that adenosine derived from astrocytes differentially regulates excitatory and inhibitory synaptic transmission in the CeM by activating specific adenosine receptors. Therefore, rather than triggering broad, unspecific effects, astrocytes exert their regulatory actions though selective interaction with specific synapses via the activation of specific signaling pathways. In addition, here we show that the synapse specificity of synaptic regulation by astrocytes has important consequences for network function and animal behavior.

Our results identify a functional role of astrocytes in the amygdala and reveal that bidirectional astrocyte–neuron communication is relevant in amygdala physiology, regulating the amygdala's functional connectivity and its behavioral outcome. Therefore, these results suggest that brain functions and their behavioral consequences result from synapse-specific signaling and the coordinated activity of astrocytes and neurons.

ONLINE METHODS

Ethics statement

All of the procedures for handling and killing animals were approved by the University of Minnesota Institutional Animal Care and Use Committee (IACUC) in compliance with the National Institutes of Health guidelines for the care and use of laboratory animals.

Animals

Mice were housed under a 12-h/12-h light/dark cycle with up to five animals per cage. Male C57BL/6J mice (14–21 d old) were used for slice electrophysiology. For specific experiments, slices were obtained from male GFAP-CB1R–null and GFAP-CB1R^{WT} mice (12–20 weeks old) and from male IP3R2^{-} mice (14–21 d old), which were generously donated by Dr. G. Marsicano and Dr. J. Chen, respectively[51, 52]. For DREADD (AAV8-GFAP-hM3D–mCherry) activation experiments, 9–20-week-old male C57BL/6J mice were used for slice electrophysiology and *in vivo* electrophysiology, and 9–12-week-old male C57BL/6J mice were used for the delayed fear conditioning and elevated plus maze experiments.

Mice carrying the 'floxed' CB1R–expressing gene (*Cnr1*$^{f/f}$) were crossed with GFAP-CreERT2 mice[53] via a three-step backcrossing procedure to produce *Cnr1*$^{f/f}$;GFAP-CreERT2 and *Cnr1*$^{f/f}$ littermates, referred to here as GFAP-CB1R–null and GFAP-CB1R^{WT} mice, respectively. CreERT2 protein is inactive in the absence of tamoxifen treatment; *Cnr1* was 'deleted' in adult mice (8 weeks old) by eight daily injections of tamoxifen (1 mg i.p.) dissolved in 90% sunflower oil, 10% ethanol to a final concentration of 10 mg/ml (ref. 53). The animals were used at least 4 weeks after tamoxifen treatment.

Amygdala slice preparation

To obtain brain slices containing the amygdaloid complex, we decapitated animals and then rapidly removed their brains and placed the brains in ice-cold artificial cerebrospinal fluid (ACSF). Slices (350 μm thick) were incubated for 1 h at room temperature (21–24 °C) in ACSF that contained 2.69 mM NaCl, 1.25 mM KH_2PO_4, 2 mM $MgSO_4$, 26 mM $NaHCO_3$, 2 mM $CaCl_2$ and 10 mM glucose and was gassed with 95% O_2, 5% CO_2, pH 7.3. Slices were then transferred to an immersion recording chamber and superfused at 2 ml/min. The chamber volume was replaced in 8–12 min with gassed ACSF. The amygdaloid complex and its different subnuclei were easily identified by transillumination with a 4× objective and use of the Allen Brain Atlas as a reference. We confirmed the location of the CeM nucleus on the basis of the neuronal electrical properties[12, 54], observing low-threshold bursting (19 out of 35 recorded neurons; 54.3%), regular spiking (10 out of 35 neurons; 28.5%), late-firing (5 out of 35 neurons; 14.3%) and stuttering neurons (1 out of 35 neurons; 2.9%).

Electrophysiology

Neurons were identified by infrared differential interference contrast microscopy. Simultaneous electrophysiological recordings from CeM neurons were obtained via the whole-cell patch-clamp technique. Patch electrodes had resistances of 3–10 MΩ when filled with an internal solution that contained 135 mM $KMeSO_4$, 10 mM KCl, 10 mM HEPES-K, 5 mM NaCl, 2.5 mM ATP-Mg^{+2}, and 0.3 mM GTP-Na^{+}, pH 7.3. The BAPTA-containing intracellular solution contained 40 mM BAPTA-K_4, 2 mM ATP-Na_2, 10 mM HEPES, 1 mM $MgCl_2$ and 8 mM NaCl, pH 7.3. To reveal the astrocyte network, we also included biocytin (0.1%) in this solution; slices were fixed and biocytin was revealed by Alexa Fluor 488–streptavidin. Recordings were obtained with PC-ONE amplifiers (Dagan Instruments, Minneapolis, MN). Fast and slow whole-cell capacitances were neutralized and series resistance was compensated (~70%), and the membrane potential was held in a range from

−70 mV to −80 mV. Electrophysiological properties were monitored during the experiments, and recordings were considered stable when the series and input resistances, resting membrane and stimulus artifact duration did not change by more than 20%. Cells that did not meet these criteria were discarded. Signals were fed to a Pentium-based PC through a DigiData 1440A interface board. Signals were filtered at 1 kHz and acquired at a 10-kHz sampling rate. The pCLAMP 10.2 (Axon Instruments) software was used for stimulus generation, data display, acquisition and storage. The distance between the somas of the paired recorded neurons was 70–150 μm.

Synaptic stimulation

Theta capillaries (2–5-μm tip) filled with ACSF were used for bipolar local stimulation. The electrodes were connected to an S-910 stimulator through an isolation unit. GABAergic IPSCs in CeM neurons were evoked by local electrical stimulation through an extracellular stimulation electrode located in the CeL, and isolated in the presence of AMPAR and NMDAR antagonists (CNQX 20 μM and D-AP5 50 μM). Glutamatergic EPSCs in CeM neurons were evoked by local electrical stimulation through an extracellular stimulation electrode located in the BLA, and isolated in the presence of $GABA_AR$ and $GABA_BR$ blockers (Picrotoxin 0.05 mM and CGP 5 μM, respectively). The synaptic responses showed failures and successes in neurotransmitter release[26, 38, 39, 55]. The stimulus parameters were adjusted to meet the conditions of putative single or very few presynaptic fibers, and remained unchanged during the experiment. Synapses that did not meet the criteria were discarded. A response was considered a success if the amplitude of the current was >3 times the s.d. of the baseline current and was verified by visual inspection. We quantified the Pr as the ratio between successes and failures in evoked synaptic transmission, and the synaptic potency as the amplitude of the successful responses. Paired pulses (250-μs duration and 50-ms interval) were continuously delivered at 0.33 Hz. The paired-pulse ratio was estimated as PPR = second EPSC/first EPSC or second IPSC/first IPSC. The average of the successes and failures was used as the amplitude of the EPSC or IPSC for this calculation.

Basal synaptic parameters were considered to be the parameters during the 5 min before the application of the stimulus. The stimulus to induce eCB release was a 10-s ND to 0 mV (ref. 35). The ND was applied 2.5 s after the last basal delivered pulse, and no pulses were presented during the ND. Immediately after the ND was finished, the 0.33-Hz pulse protocol was started again. For acute application of CNO, a micropipette was filled with 1 mM CNO solution and placed 100–150 μm away from the recording neuron, and a pressure pulse was applied for 2 s. The absence of mechanical movement of the tissue was confirmed in every case. In the text, data are expressed as a percentage relative to the basal 5 min. Results were compared by two-tailed Student's paired *t*-test unless otherwise stated.

Ca^{2+} imaging

Ca^{2+} levels in astrocytes located in the CeM were monitored by fluorescence microscopy with the Ca^{2+} indicator fluo-4 (Molecular Probes, Eugene, OR). Slices were incubated with fluo-4 AM (2 μl of 2 mM dye were dropped over the amygdaloid complex, yielding a final concentration of 2 μM and 0.01% pluronic) for 20–30 min at room temperature. In these conditions, most of the cells loaded were astrocytes, as confirmed by their

electrophysiological properties and SR101 staining[33, 56]. SR101 was intraperitoneally injected (100 mg/kg) and the animal was left in the cage for ~30–45 min until intense coloration was observed in paws and ears, as reported[57]. With this staining procedure SR101 stains specifically astrocytes[56–58] (but see ref. 59). Astrocytes were imaged either with a CCD (charge-coupled device) camera (Retiga EX, Qimaging, Canada) attached to the Olympus microscope or in a multiphoton scope Leica SP5. Cells were illuminated for 100 ms with an LED at 488 nm, and images were acquired every 1 s. Intracellular Ca^{2+} signals were monitored from CeM astrocytes, and Ca^{2+} variations were recorded at the soma and proximal processes. The signal was measured as fluorescence over baseline ($\Delta F/F_0$), and cells were considered to have displayed a calcium event when the $\Delta F/F_0$ of the calcium signal increased by three times the s.d. of the baseline for at least two consecutive images.

The astrocyte Ca^{2+} signal was quantified as the probability of occurrence of a Ca^{2+} event (calcium event probability). The Ca^{2+} event probability was calculated as the number of astrocytes starting a calcium event per time bin in a field of view, divided by the number of astrocytes in that field of view (10–20 astrocytes). The calcium event probability was calculated in each slice, and for statistical analysis the sample size corresponded to the number of slices, because different slices were considered as independent variables. Events were grouped in 10-s time bins. The time of occurrence of an event was considered to be at the onset of the Ca^{2+} event. To test the effects of the different stimuli, we compared the respective mean basal calcium event probability with the calcium event probability in the time bin after the stimulus. Mean values were obtained from at least four slices in each condition. For the CNO perfusion, the Ca^{2+} signal was quantified as a calcium event frequency; thus it was calculated as the number of calcium events each astrocyte displayed per minute in a field of view. The calcium event frequency was grouped in time bins of 1 min. To test the effect of CNO perfusion, we compared the basal calcium event frequency to the calcium event frequency 4 and 5 min after the initial CNO application.

Virus delivery of DREADDs and confirmation of virus expression location

AAV8-GFAP-hM3D–mCherry (adenovirus serotype 8, 2×10^{12} virus molecules per ml; Gene Therapy Vector Core at University of North Carolina) was used. Stereotaxic bilateral injections (300–500 nl at 100 nl min^{-1}) were made into the CeM (anterior–posterior, −1 mm; medial–lateral, ±2.75 mm; dorsa–lventral, 5.15 mm; from bregma) of C57BL/6J mice at 6–9 weeks of age. Three weeks after the virus injection, the location of the virus was confirmed on the basis of mCherry expression. Only animals in which the expression was located mainly in the CeM, with no major leak into other subnuclei, were used. Animals in which the expression did not meet these location criteria were discarded.

Immunohistochemistry

Anesthetized C57BL/6J mice transfected with AAV8-GFAP-hM3D–mCherry were perfused intracardially with 0.1 M PBS followed by 4% paraformaldehyde ($n = 6$ mice). Brains were extracted and post-fixed in paraformaldehyde overnight. Each brain was sectioned into 50-μm slices that were then blocked in 10% normal goat serum with 0.1% Triton X-100 in PBS (1 h, room temperature) and stained for rabbit GFAP-specific antibody (1:1,000; Sigma; G9269), mouse NeuN-specific antibody (1:500; Millipore; MAB377), rabbit NeuN-specific

antibody[60] (1:500; Millipore; MABN140), mouse NG2-specific antibody[61] (1:500; Millipore; AB5320), rabbit Iba1 antibody[62] (1:500; Dako; 019–19741), and mouse CC1-specific antibody[63] (1:500; Calbiochem; OP80) overnight (4 °C). This was followed by a 3-h incubation in Alexa Fluor 488 goat anti-rabbit (1:500; Invitrogen; A11034), Alexa Fluor 405 goat anti-mouse (1:500; Invitrogen; A31553) and Cy3 goat anti-mouse (1:500) before being mounted on a glass slide with Vectashield Hardset mounting media (Vector Labs). Detailed information regarding antibody validation is included in the **Life Sciences Reporting Summary**. The slides were imaged with a Leica SP5 multiphoton confocal microscope. The cellular specificity of DREADD expression was tested by immunohistochemical analysis of randomly selected areas of CeM. Out of 790 DREADD-expressing cells (assessed by mCherry fluorescence), 785 cells (99.36%) were identified as astrocytes on the basis of their colocalization with GFAP, 3 cells (0.37%) were neurons (identified by colocalization with NeuN), 2 cells (0.25%) were oligodendrocytes (identified by colocalization with CC1), and none (0.0%) were microglia (identified by colocalization with Iba1) or oligodendrocyte precursor cells (identified by colocalization with NG2). Moreover, 88.1% of astrocytes identified by GFAP (785 out of 891 astrocytes; 15 slices; 6 mice), 1.1% of oligodendrocytes identified by CC1 (2 out of 173 oligodendrocytes; 6 slices; 2 mice), 0.11% of neurons identified by NeuN (3 out of 2,596; 19 slices; 6 mice), 0.0% of microglia identified by Iba1 (0 out of 178; 9 slices; 2 mice) and 0.0% oligodendrocyte precursor cells identified by NG2 (0 out of 100; 9 slices; 3 mice) expressed DREADDs (monitored by mCherry expression). These results indicate that the number of cells other than astrocytes that expressed DREADDs was negligible (0.6%) and that a vast amount (88.1%) of CeM astrocytes expressed DREADDs.

The above-described selective GFAP-driven DREADD expression in CeM astrocytes supports the specific deletion of astrocytic CB1R in GFAP-CB1R–null mice. To directly test this idea, we analyzed the functional expression of CB1R. Neuronal expression of CB1R was assessed on the basis of the depolarization-induced suppression of inhibition (DSI), a well-characterized purely neuronal phenomenon dependent on presynaptic CB1R[35, 36, 64], and astrocyte expression of CB1R was assessed on the basis of CB1R–mediated Ca^{2+} elevations evoked by neuronal depolarization[32, 38]. We found that in wild-type mice neuronal depolarization evoked both DSI and increases in amounts of astrocyte Ca^{2+}, whereas in GFAP-CB 1R–null mice the DSI was still present but the increase in astrocyte Ca^{2+} was absent (Supplementary Fig. 9). These results show that in GFAP-CB1R–mice, CB1R–mediated signaling was selectively abolished in astrocytes, whereas CB1R–mediated signaling was preserved in neurons, indicating the specific deletion of CB1R in astrocytes.

For astrocytic network labeling, after biocytin filling, slices were fixed in 4% PFA in 0.1 PBS, pH 7.4, at 4 °C. Biocytin was visualized with Alexa Fluor 488-streptavidin (RRID AB_2315383; 1:500).

In vivo electrophysiological recordings

Mice were anesthetized (urethane, 1.8 g/kg i.p.) and placed in a stereotaxic frame (ASI Instruments). Their body temperature was maintained at 37 ± 1 °C with a heating blanket, and breathing rates were constantly monitored. A tungsten electrode (5-MΩ impedance at

1,000 Hz) for electrophysiological recordings of multi-unit activity was located stereotaxically in the same coordinates as for virus injection for each animal (anterior–posterior, −1 mm; medial–lateral, ±2.75 mm; dorsal-ventral, −5.15 mm; from bregma). The signal was amplified and filtered (300-3,000 Hz) with a differential amplifier (Model 3000 AC/DC, AM System). Signals were digitalized at 10 KHz with an A/D converter (DigiData 1550A, Axons Instruments) and stored in a PC for posterior analysis with the software pCLAMP 10.2 (Axon Instruments). Spikes were detected in offline analysis with the following criteria: a voltage threshold was located at the level of the average of background noise plus three times the s.d. (obtained during long silent periods) and verified by visual inspection. In every mouse, spikes were grouped in clusters on the basis of spike amplitude. A scalp vein set was filled with either saline or CNO (2 mg/kg) and was placed intraperitoneally before the recording started. After 30 min of baseline recording, either CNO or saline was applied.

Delayed fear conditioning

This associative learning task involved measuring a fear response (i.e., time spent freezing) to a conditioned stimulus (cue) that was predictive of an unconditioned stimulus (mild foot shock) presented during training trials. Data collection and analysis were semi-automated via a video-monitoring fear-conditioning apparatus (Med Associates, Inc.). On the conditioning day (training day), mice were exposed to a series (five pairings; 60-s intertrial interval) of cue (80-dB white noise tone and light) presentations (15 s in duration) that co-terminated with a mild foot shock (0.7 mA, 1 s in duration). Twenty-four hours later mice were injected with either CNO (2 mg/kg i.p.) or saline 30 min before the first cued fear test (test day 1). Cued fear testing took place in a test chamber with altered contextual elements (floor, wall and odor) and consisted of a 3-min baseline (nonspecific freezing behavior) and a 3-min cue exposure (cued fear) period. This cued fear test was then repeated 24 h later (test day 2) without any CNO exposure. Freezing response was assessed during the various procedural components of both the conditioning (conditioned stimulus and intertrial interval) and testing (baseline and cue) sessions. For the memory tests, we broke freezing down further into 1-min time bins within each session to investigate within-session changes.

Elevated plus maze

Subjects were tested on an elevated plus maze (EPM) apparatus (Med Associates, Inc.). Testing was done under dim lighting conditions, with low-intensity LED lights over the open arms generating ~50 lx of brightness at the end of the arms. Tests were 5 min in duration, and movement was tracked and analyzed with ANY-maze software (Stoelting Co.). Open arm time (as a percentage of total arm exploration), open and closed arm entries and total distance traveled were determined by the software. Mice were injected with either CNO (2 mg/kg i.p.) or saline 30 min before the test. The same subjects were used in the EPM testing as were used for fear conditioning. The EPM test was performed 1 week after fear testing, and the CNO/saline treatments were assigned randomly, irrespective of previous exposure.

Drugs and chemicals

N-(piperidin-1-yl)-5-(4-iodophenyl)-1-(2,4-dichlorophenyl)-4-methyl-1H–pyrazole-3-carboxamide (AM251), 2-methyl-6-(phenylethynyl)pyridine hydrochloride (MPEP), (S)-(+)-

α-amino-4-carboxy-2-methylbenzeneacetic acid (LY367385 (LY)), and (2*S*)-3-[[(1*S*)-1-(3,4-dichlorophenyl)ethyl]amino-2-hydroxypropyl](phenylmethyl)phosphonic acid hydrochloride (CGP 55845) were purchased from Tocris Cookson (Bristol, UK); Fluo-4 AM (Eugene, OR) and picrotoxin were from Indofine Chemical Company (Hillsborough, NJ). BAPTA tetrapotassium salt was from Thermo Fisher Scientific (Waltham, MA). All other drugs were purchased from Sigma.

Statistical analysis

The normality and equal variance tests were performed before the application of statistical comparisons, which were made by parametric Student's *t*-test unless otherwise stated. Data are expressed as mean ± s.e.m. unless otherwise stated. To analyze the effects of the stimulus in the same synapse, we used paired Student's *t*-test to compare values before and after the stimulus. To analyze the effects of different treatments and conditions, we carried out multiple comparison testing between the different groups. Therefore, results were compared by either a two-tailed Student's *t*-test ($\alpha = 0.05$) or a two-way ANOVA using the 'basal' and the 'post-stimulus' situations as factor 1 and the different experimental conditions as factor 2. The *post hoc* test used was Holm–Sidak, versus control comparisons, corrected for multiple comparisons, always using the 'basal' situation and the 'control' condition as the controls to compare. Statistical differences were established with $^{*}P < 0.05$, $^{**}P < 0.01$ and $^{***}P < 0.001$ for Student's *t*-test or with $^{\#}P < 0.05$, $^{\#\#}P < 0.01$ and $^{\#\#\#}P < 0.001$ for the *post hoc* Holm–Sidak test. For detailed information see Supplementary Tables 1 and 3–5. No animals or data points were excluded from the analysis. Data collection and analysis were not performed with blinding to the condition of the experiments, but the same criteria were applied to all allocated groups for comparisons. Randomization was not used. No statistical methods were used to predetermine sample sizes, but our sample sizes were similar to those generally used in the field[26, 36, 64].

Data availability

The data that support the findings of this study are available from the corresponding author on reasonable request.

Supplementary Material

Refer to Web version on PubMed Central for supplementary material.

Acknowledgments

We thank J. Chen (UCSD, La Jolla, California, USA) for providing IP3R2^{-} mice, and W. Buño, G. Perea, M. Navarrete and A. Covelo for helpful comments. This work was supported by NIH–NINDS (R01NS097312-01 to A.A.), the Human Frontier Science Program (Research Grant RGP0036/2014 to A.A. and G.M.), INSERM (to G.M.), Fondation pour la Recherche Medicale (DRM20101220445 to G.M.) and the China Scholarship Council (to Z.Z.). We thank the MnDRIVE Optogenetics Core at the University of Minnesota for technical support, and B. Roth and the UNC Vector Core (Chapel Hill, North Carolina, USA) for providing the Gq-DREADD adeno-associated virus.

References

1. LeDoux JE. Emotion circuits in the brain. Annu. Rev. Neurosci. 2000; 23:155–184. [PubMed: 10845062]
2. Duvarci S, Pare D. Amygdala microcircuits controlling learned fear. Neuron. 2014; 82:966–980. [PubMed: 24908482]
3. Ehrlich I, et al. Amygdala inhibitory circuits and the control of fear memory. Neuron. 2009; 62:757–771. [PubMed: 19555645]
4. McDonald AJ. Neurons of the lateral and basolateral amygdaloid nuclei: a Golgi study in the rat. J. Comp. Neurol. 1982; 212:293–312. [PubMed: 6185547]
5. LeDoux JE, Farb C, Ruggiero DA. Topographic organization of neurons in the acoustic thalamus that project to the amygdala. J. Neurosci. 1990; 10:1043–1054. [PubMed: 2158523]
6. McDonald AJ. Cortical pathways to the mammalian amygdala. Prog. Neurobiol. 1998; 55:257–332. [PubMed: 9643556]
7. McDonald AJ. Cytoarchitecture of the central amygdaloid nucleus of the rat. J. Comp. Neurol. 1982; 208:401–418. [PubMed: 7119168]
8. LeDoux JE, Iwata J, Cicchetti P, Reis DJ. Different projections of the central amygdaloid nucleus mediate autonomic and behavioral correlates of conditioned fear. J. Neurosci. 1988; 8:2517–2529. [PubMed: 2854842]
9. Tovote P, et al. Midbrain circuits for defensive behaviour. Nature. 2016; 534:206–212. [PubMed: 27279213]
10. Li H, et al. Experience-dependent modifcation of a central amygdala fear circuit. Nat. Neurosci. 2013; 16:332–339. [PubMed: 23354330]
11. Penzo MA, et al. The paraventricular thalamus controls a central amygdala fear circuit. Nature. 2015; 519:455–459. [PubMed: 25600269]
12. Haubensak W, et al. Genetic dissection of an amygdala microcircuit that gates conditioned fear. Nature. 2010; 468:270–276. [PubMed: 21068836]
13. Ciocchi S, et al. Encoding of conditioned fear in central amygdala inhibitory circuits. Nature. 2010; 468:277–282. [PubMed: 21068837]
14. Amano T, Unal CT, Paré D. Synaptic correlates of fear extinction in the amygdala. Nat. Neurosci. 2010; 13:489–494. [PubMed: 20208529]
15. Tye KM, et al. Amygdala circuitry mediating reversible and bidirectional control of anxiety. Nature. 2011; 471:358–362. [PubMed: 21389985]
16. Viviani D, et al. Oxytocin selectively gates fear responses through distinct outputs from the central amygdala. Science. 2011; 333:104–107. [PubMed: 21719680]
17. Araque A, et al. Gliotransmitters travel in time and space. Neuron. 2014; 81:728–739. [PubMed: 24559669]
18. Araque A, Parpura V, Sanzgiri RP, Haydon PG. Tripartite synapses: glia, the unacknowledged partner. Trends Neurosci. 1999; 22:208–215. [PubMed: 10322493]
19. Fields RD, et al. Glial biology in learning and cognition. Neuroscientist. 2014; 20:426–431. [PubMed: 24122821]
20. Perea G, Navarrete M, Araque A. Tripartite synapses: astrocytes process and control synaptic information. Trends Neurosci. 2009; 32:421–431. [PubMed: 19615761]
21. Araque A, Martin ED, Perea G, Arellano JI, Buno W. Synaptically released acetylcholine evokes Ca^{2+} elevations in astrocytes in hippocampal slices. J. Neurosci. 2002; 22:2443–2450. [PubMed: 11923408]
22. Di Castro MA, et al. Local Ca^{2+} detection and modulation of synaptic release by astrocytes. Nat. Neurosci. 2011; 14:1276–1284. [PubMed: 21909085]
23. Volterra A, Liaudet N, Savtchouk I. Astrocyte Ca^{2+} signalling: an unexpected complexity. Nat. Rev. Neurosci. 2014; 15:327–335. [PubMed: 24739787]
24. Parri HR, Gould TM, Crunelli V. Spontaneous astrocytic Ca^{2+} oscillations in situ drive NMDAR-mediated neuronal excitation. Nat. Neurosci. 2001; 4:803–812. [PubMed: 11477426]

25. Henneberger C, Papouin T, Oliet SH, Rusakov DA. Long-term potentiation depends on release of D-serine from astrocytes. Nature. 2010; 463:232–236. [PubMed: 20075918]
26. Perea G, Araque A. Astrocytes potentiate transmitter release at single hippocampal synapses. Science. 2007; 317:1083–1086. [PubMed: 17717185]
27. Panatier A, et al. Astrocytes are endogenous regulators of basal transmission at central synapses. Cell. 2011; 146:785–798. [PubMed: 21855979]
28. Oliveira JF, Sardinha VM, Guerra-Gomes S, Araque A, Sousa N. Do stars govern our actions? Astrocyte involvement in rodent behavior. Trends Neurosci. 2015; 38:535–549. [PubMed: 26316036]
29. Scofeld MD, et al. Gq-DREADD selectively initiates glial glutamate release and inhibits cue-induced cocaine seeking. Biol. Psychiatry. 2015; 78:441–451. [PubMed: 25861696]
30. Han J, et al. Acute cannabinoids impair working memory through astroglial CB1 receptor modulation of hippocampal LTD. Cell. 2012; 148:1039–1050. [PubMed: 22385967]
31. Halassa MM, et al. Astrocytic modulation of sleep homeostasis and cognitive consequences of sleep loss. Neuron. 2009; 61:213–219. [PubMed: 19186164]
32. Navarrete M, Araque A. Endocannabinoids mediate neuron-astrocyte communication. Neuron. 2008; 57:883–893. [PubMed: 18367089]
33. Martín R, Bajo-Grañeras R, Moratalla R, Perea G, Araque A. Circuit-specifc signaling in astrocyte-neuron networks in basal ganglia pathways. Science. 2015; 349:730–734. [PubMed: 26273054]
34. Min R, Nevian T. Astrocyte signaling controls spike timing-dependent depression at neocortical synapses. Nat. Neurosci. 2012; 15:746–753. [PubMed: 22446881]
35. Kamprath K, et al. Short-term adaptation of conditioned fear responses through endocannabinoid signaling in the central amygdala. Neuropsychopharmacology. 2011; 36:652–663. [PubMed: 20980994]
36. Ramikie TS, et al. Multiple mechanistically distinct modes of endocannabinoid mobilization at central amygdala glutamatergic synapses. Neuron. 2014; 81:1111–1125. [PubMed: 24607231]
37. Agulhon C, Fiacco TA, McCarthy KD. Hippocampal short- and long-term plasticity are not modulated by astrocyte Ca^{2+} signaling. Science. 2010; 327:1250–1254. [PubMed: 20203048]
38. Navarrete M, Araque A. Endocannabinoids potentiate synaptic transmission through stimulation of astrocytes. Neuron. 2010; 68:113–126. [PubMed: 20920795]
39. Raastad M, Storm JF, Andersen P. Putative single quantum and single fbre excitatory postsynaptic currents show similar amplitude range and variability in rat hippocampal slices. Eur. J. Neurosci. 1992; 4:113–117. [PubMed: 12106447]
40. Dunwiddie TV, Diao L. Extracellular adenosine concentrations in hippocampal brain slices and the tonic inhibitory modulation of evoked excitatory responses. J. Pharmacol. Exp. Ther. 1994; 268:537–545. [PubMed: 8113965]
41. Pascual O, et al. Astrocytic purinergic signaling coordinates synaptic networks. Science. 2005; 310:113–116. [PubMed: 16210541]
42. Panatier A, et al. Glia-derived D-serine controls NMDA receptor activity and synaptic memory. Cell. 2006; 125:775–784. [PubMed: 16713567]
43. Sherwood MW, et al. Astrocytic IP3 Rs: contribution to Ca^{2+} signalling and hippocampal LTP. Glia. 2017; 65:502–513. [PubMed: 28063222]
44. Perea G, et al. Activity-dependent switch of GABAergic inhibition into glutamatergic excitation in astrocyte-neuron networks. eLife. 2016; 5:e20362. [PubMed: 28012274]
45. Serrano A, Haddjeri N, Lacaille JC, Robitaille R. GABAergic network activation of glial cells underlies hippocampal heterosynaptic depression. J. Neurosci. 2006; 26:5370–5382. [PubMed: 16707789]
46. Poskanzer KE, Yuste R. Astrocytes regulate cortical state switching in vivo. Proc. Natl. Acad. Sci. USA. 2016; 113:E2675–E2684. [PubMed: 27122314]
47. Gómez-Gonzalo M, et al. Endocannabinoids induce lateral long-term potentiation of transmitter release by stimulation of gliotransmission. Cereb. Cortex. 2015; 25:3699–3712. [PubMed: 25260706]

48. Castillo PE, Younts TJ, Chávez AE, Hashimotodani Y. Endocannabinoid signaling and synaptic function. Neuron. 2012; 76:70–81. [PubMed: 23040807]
49. Kano M, Ohno-Shosaku T, Hashimotodani Y, Uchigashima M, Watanabe M. Endocannabinoid-mediated control of synaptic transmission. Physiol. Rev. 2009; 89:309–380. [PubMed: 19126760]
50. Covelo A, Araque A. Lateral regulation of synaptic transmission by astrocytes. NeuroScience. 2016; 323:62–66. [PubMed: 25732135]
51. Zimmer A, Zimmer AM, Hohmann AG, Herkenham M, Bonner TI. Increased mortality, hypoactivity, and hypoalgesia in cannabinoid CB1 receptor knockout mice. Proc. Natl. Acad. Sci. USA. 1999; 96:5780–5785. [PubMed: 10318961]
52. Li X, Zima AV, Sheikh F, Blatter LA, Chen J. Endothelin-1-induced arrhythmogenic Ca^{2+} signaling is abolished in atrial myocytes of inositol-1,4,5-trisphosphate (IP3)-receptor type 2-defcient mice. Circ. Res. 2005; 96:1274–1281. [PubMed: 15933266]
53. Hirrlinger PG, Scheller A, Braun C, Hirrlinger J, Kirchhoff F. Temporal control of gene recombination in astrocytes by transgenic expression of the tamoxifen-inducible DNA recombinase variant CreERT2. Glia. 2006; 54:11–20. [PubMed: 16575885]
54. Dumont EC, Martina M, Samson RD, Drolet G, Paré D. Physiological properties of central amygdala neurons: species differences. Eur. J. Neurosci. 2002; 15:545–552. [PubMed: 11876782]
55. Braga MF, Aroniadou-Anderjaska V, Xie J, Li H. Bidirectional modulation of GABA release by presynaptic glutamate receptor 5 kainate receptors in the basolateral amygdala. J. Neurosci. 2003; 23:442–452. [PubMed: 12533604]
56. Perez-Alvarez A, Navarrete M, Covelo A, Martin ED, Araque A. Structural and functional plasticity of astrocyte processes and dendritic spine interactions. J. Neurosci. 2014; 34:12738–12744. [PubMed: 25232111]
57. Pérez-Alvarez A, Araque A, Martín ED. Confocal microscopy for astrocyte in vivo imaging: recycle and reuse in microscopy. Front. Cell. Neurosci. 2013; 7:51. [PubMed: 23658537]
58. Appaix F, et al. Specifc in vivo staining of astrocytes in the whole brain after intravenous injection of sulforhodamine dyes. PLoS One. 2012; 7:e35169. [PubMed: 22509398]
59. Hagos L, Hülsmann S. Unspecifc labelling of oligodendrocytes by sulforhodamine 101 depends on astrocytic uptake via the thyroid hormone transporter OATP1C1 (SLCO1C1). Neurosci. Lett. 2016; 631:13–18. [PubMed: 27519929]
60. Kim KK, Adelstein RS, Kawamoto S. Identifcation of neuronal nuclei (NeuN) as Fox-3, a new member of the Fox-1 gene family of splicing factors. J. Biol. Chem. 2009; 284:31052–31061. [PubMed: 19713214]
61. Rolls A, et al. Toll-like receptors modulate adult hippocampal neurogenesis. Nat. Cell Biol. 2007; 9:1081–1088. [PubMed: 17704767]
62. Imai Y, Ibata I, Ito D, Ohsawa K, Kohsaka S. A novel gene *iba1* in the major histocompatibility complex class III region encoding an EF hand protein expressed in a monocytic lineage. Biochem. Biophys. Res. Commun. 1996; 224:855–862. [PubMed: 8713135]
63. Bhat RV, et al. Expression of the APC tumor suppressor protein in oligodendroglia. Glia. 1996; 17:169–174. [PubMed: 8776583]
64. Wilson RI, Nicoll RA. Endogenous cannabinoids mediate retrograde signalling at hippocampal synapses. Nature. 2001; 410:588–592. [PubMed: 11279497]

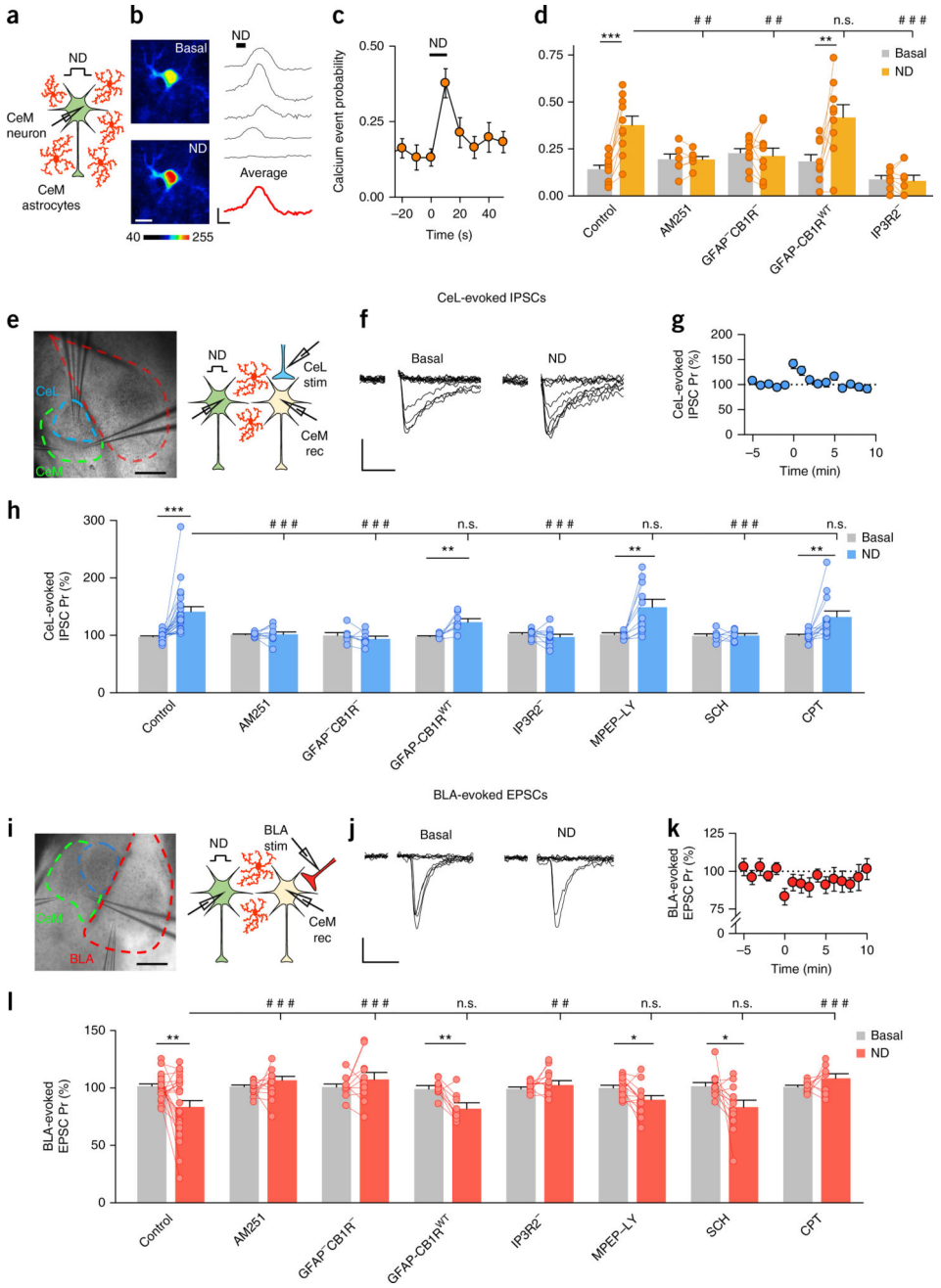

Figure 1.

Endogenously mobilized eCBs mediate CB1R–dependent increases in astrocytic calcium levels, enhance inhibitory synaptic transmission in CeL–CeM synapses and depress excitatory synaptic transmission in BLA–CeM synapses. (**a**) A schematic representation of the experimental design. (**b**) Left, pseudocolor images showing fluorescence intensities in CeM astrocytes before and after ND. Scale bar, 10 μm. Right, astrocytic calcium levels before and after ND (black), and an averaged trace of astrocytes in the field of view (red). Scale bars, 50% and 10 s for the individual traces (black), and 20% and 10 s for the average trace (red). (**c**) Calcium event probability before and after ND at time 0 (n = 10). (**d**)

Calcium event probability before and after ND in control conditions ($n = 10$; $P > 0.001$); in the presence of AM251 ($n = 7$; $P = 0.96$); and in GFAP-CB1R–null ($n = 9$; $P = 0.54$), GFAP-CB1R^{WT} ($n = 10$; $P = 0.006$) and IP3R2 ($n = 8$; $P = 0.73$) mice. The increase observed in the control condition was abolished in the presence of AM251 ($P < 0.001$) and in GFAP-CB1R–null ($P = 0.004$) and IP3R2 mice ($P = 0.003$), but not in the GFAP-CB1^{WT} mice ($P = 0.421$; two-way ANOVA, *post hoc* Holm–Sidak corrected for four comparisons). (**e**) Left, an infrared differential interference contrast microscopy (DIC) image showing the stimulation pipette in the CeL subnucleus and two recording pipettes in the CeM subnucleus. Scale bar, 250 μm. Right, a scheme of the experimental approach for obtaining recordings (rec) in the CeM from the homoneuron (green) and the heteroneuron (yellow) and the stimulation (stim) of GABAergic inputs from the CeL (blue). (**f**) IPSCs evoked by CeL stimulation recorded in the CeM heteroneuron, in basal conditions and after CeM homoneuron ND. Scale bars, 10 pA and 25 ms. (**g**) CeL-evoked IPSC Pr before and after homoneuron ND (at time 0; $n = 22$). (**h**) CeL-evoked IPSC Pr before and after homoneuron ND in control conditions ($n = 22$; $P < 0.001$); in the presence of AM251 ($n = 11$; $P = 0.74$); in GFAP-CB1R–null ($n = 7$; $P = 0.21$), GFAP-CB1R^{WT} ($n = 7$; $P = 0.008$) and IP3R2 ($n = 10$; $P = 0.03$) mice; and in the presence of MPEP + LY ($n = 10$; $P = 0.0038$), SCH ($n = 7$; $P = 0.22$) and CPT ($n = 13$; $P = 0.006$). The ND-evoked increase in Pr was prevented in the presence of AM251 ($P < 0.001$) or SCH ($P < 0.001$), and in GFAP-CB1R–null ($P < 0.001$) and IP3R2 ($P < 0.001$) mice, but was unaffected in the presence of MPEP + LY ($P = 0.35$) or CPT ($P = 0.45$) and in GFAP-CB1^{WT} mice ($P = 0.18$; two-way ANOVA, *post hoc* Holm–Sidak corrected for seven comparisons). (**i**) Left, a DIC image showing the stimulation pipette in the BLA subnucleus and two recording pipettes in the CeM subnucleus. Scale bar, 250 μm. Right, a scheme of the experimental approach for obtaining recordings in CeM from the homoneuron (green) and the heteroneuron (yellow) and the stimulation of excitatory inputs from BLA (red). (**j**) EPSCs evoked by BLA stimulation recorded in the CeM heteroneuron, in basal conditions and after homoneuron ND. Scale bars, 10 pA and 25 ms. (**k**) BLA-evoked EPSC Pr before and after homoneuron ND (at time 0; $n = 24$). (l) BLA-evoked EPSC Pr before and after homoneuron ND in control conditions ($n = 24$; $P = 0.004$); in the presence of AM251 ($n = 12$; $P = 0.66$); in GFAP-CB1R–null ($n = 9$; $P = 0.25$), GFAP-CB1R^{WT} ($n = 11$; $P = 0.003$) and IP3R2 ($n = 10$; $P = 0.17$) mice; and in the presence of MPEP + LY ($n = 13$; $P = 0.01$), SCH ($n = 12$; $P = 0.04$) and CPT ($n = 9$; $P = 0.14$). The ND-evoked decrease in Pr was prevented in the presence of AM251 ($P < 0.001$) or CPT ($P < 0.001$) and in GFAP-CB1R–null ($P < 0.001$) and IP3R2 ($P < 0.001$) mice, but was unaffected in the presence of MPEP + LY ($P = 0.46$) or SCH ($P = 0.96$) and in GFAP-CB1^{WT} mice ($P = 0.98$; two-way ANOVA, *post hoc* Holm–Sidak corrected for seven comparisons). *$P < 0.05$, **$P < 0.01$, ***$P < 0.001$; Student's paired *t*-test. $^{\#\#}P < 0.01$, $^{\#\#\#}P < 0.001$; two-way ANOVA with *post hoc* Holm–Sidak; n.s., nonsignificant ($P > 0.05$). Data in **c,d,g,h,k,l** are mean ± s.e.m.

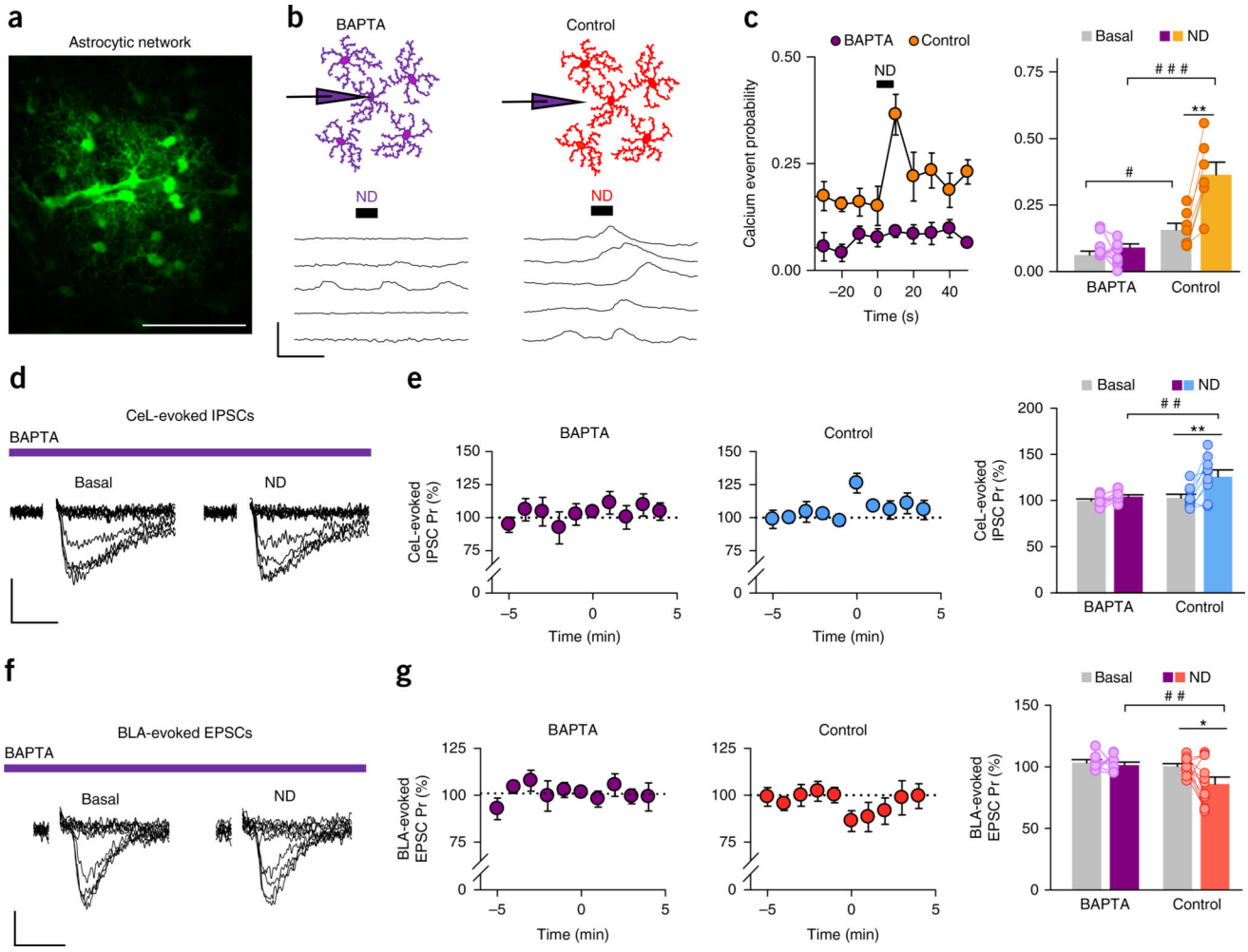

Figure 2.

Astrocytic CB1R regulation of synaptic transmission relays on astrocytic calcium activity. (**a**) A network of coupled astrocytes after a single astrocyte was filled with biocytin. Scale bar, 70 μm. (**b**) Left, a schematic representation of the experimental condition: an astrocyte was filled with BAPTA-containing intracellular solution, and the astrocyte was kept patched long enough to allow the BAPTA to diffuse to neighboring astrocytes. The traces show the changes in calcium levels in response to ND in this condition. Right, a schematic representation of the control condition: a pipette with BAPTA-containing intracellular solution was placed in the extracellular space. The traces show changes in calcium levels in response to ND in this condition. Scale bars, 20 s and 50%. (**c**) Left, calcium event probability before and after ND at time 0 in BAPTA ($n = 9$) and control ($n = 7$) conditions. Right, calcium event probability before and after ND in BAPTA ($n = 9$; $P = 0.16$) and control conditions ($n = 7$; $P < 0.001$). We observed a difference in the calcium event probability between control and BAPTA conditions both before and after ND (two-way ANOVA indicated a significant effect of ND ($P < 0.001$) and an interaction with the experimental condition ($P = 0.002$); *post hoc* Holm–Sidak corrected for two comparisons; difference between control and BAPTA before ND ($P = 0.016$) and after ND ($P < 0.001$)). (**d**) IPSCs evoked by CeL stimulation in the CeM heteroneuron in BAPTA conditions before

and after CeM homoneuron ND. Scale bars, 9 pA and 25 ms. (**e**) CeL-evoked IPSC Pr before and after homoneuron ND (at time 0) in BAPTA ($n = 8$; $P = 0.16$) and control conditions ($n = 9$; $P = 0.003$). We observed a difference in the post-ND state between the BAPTA and control conditions (two-way ANOVA indicated a significant effect of ND ($P = 0.003$) and an interaction with the experimental condition ($P = 0.038$); *post hoc* Holm–Sidak $P = 0.002$). (**f**) EPSCs evoked by BLA stimulation in the CeM heteroneuron in the BAPTA condition before and after homoneuron ND. Scale bars, 5 pA and 25 ms. (**g**) BLA-evoked EPSC Pr before and after homoneuron ND (at time 0) in BAPTA ($n = 8$; $P = 0.63$) and control ($n = 11$; $P = 0.03$) conditions. We observed a difference in the post-ND state between the BAPTA and control conditions (two-way ANOVA indicated a significant effect of ND ($P = 0.037$) and interaction with the experimental condition ($P = 0.106$); *post hoc* Holm–Sidak $P = 0.007$). $^{*}P < 0.05$, $^{**}P < 0.01$; Student's paired *t*-test. $^{\#}P < 0.05$, $^{\#\#}P < 0.01$, $^{\#\#\#}P < 0.001$; two-way ANOVA, *post hoc* Holm–Sidak. Data in **c,e,g** are mean ± s.e.m.

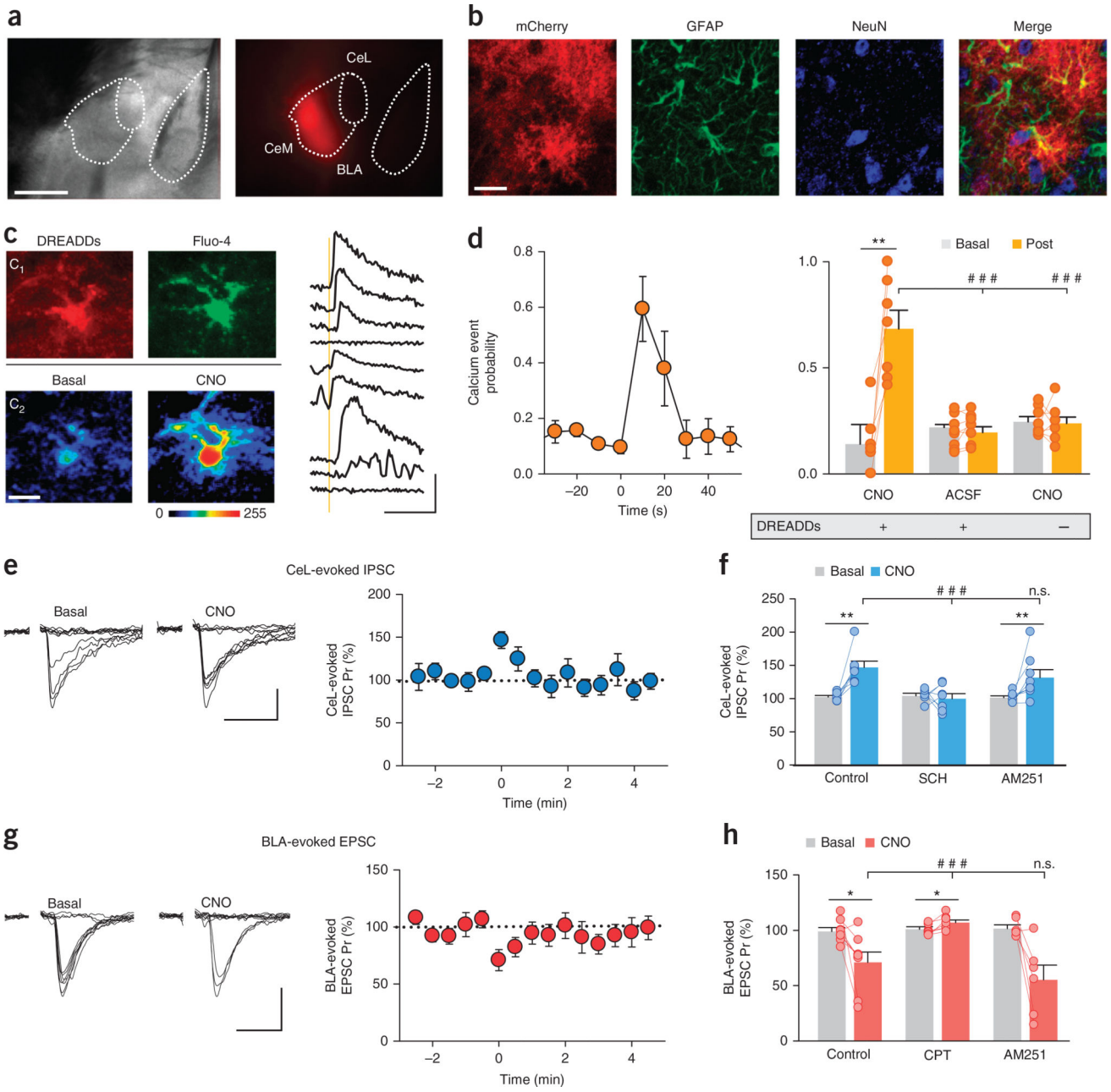

Figure 3.

Selective expression and activation of astrocytic Gq-DREADDs in the CeM increases astrocytic calcium levels, increases inhibitory synaptic transmission at CeL–CeM synapses and depresses excitatory synaptic transmission at BLA–CeM synapses. (**a**) DIC and fluorescence images showing the localization of DREADDs in the CeM as reported by mCherry expression (red). Scale bar, 500 μm. (**b**) Confocal images of mCherry labeling; astrocytes are immunohistochemically labeled with the astrocytic marker GFAP, and neurons are labeled with the neuronal marker NeuN. Scale bar, 20 μm. (**c**) Left, images of CeM astrocytes. Top, C_1 fluorescence images showing mCherry and Fluo-4. Bottom, C_2 pseudocolor images of fluorescence intensities before and after local application of CNO.

Scale bar, 5 μm. Right, astrocytic calcium levels before and after CNO application (vertical yellow bar). Scale bars, 50% and 30 s. (**d**) Left, calcium event probability in basal conditions and after CNO application at time 0 ($n = 7$). Right, calcium event probability before and after CNO application in DREADD-expressing slices ($n = 7$; $P = 0.0018$), before and after ACSF application in DREADD-expressing slices ($n = 8$; $P = 0.17$), and before and after CNO application in slices with no DREADD expression ($n = 8$; $P = 0.83$). The increase in calcium event probability observed after local application of CNO in DREADD-expressing animals was absent after local application of either ACSF or CNO in mice without DREADD expression (two-way ANOVA indicated a significant effect of CNO ($P < 0.001$) and interaction with the experimental condition ($P < 0.001$); *post hoc* Holm–Sidak-corrected for two comparisons; $P < 0.001$ in both cases). (**e**) Left, CeL-evoked IPSCs recorded in CeM neurons before and after CNO application. Scale bars, 10 pA and 25 ms. Right, CeL-evoked IPSC Pr before and after CNO application (time 0; $n = 7$). (**f**) CeL-evoked IPSC Pr before and after CNO application in control conditions ($n = 7$; $P = 0.004$) and in the presence of SCH ($n = 7$; $P = 0.96$) and AM251 ($n = 8$; $P = 0.003$). We observed a difference in the response to CNO between the control condition and the SCH condition (two-way ANOVA indicated a significant effect of CNO ($P < 0.001$) and interaction with the experimental condition ($P < 0.001$); *post hoc* Holm–Sidak-corrected for two comparisons ($P < 0.001$)) but not between control and AM251 conditions ($P = 0.12$). (**g**) Left, BLA-evoked EPSCs recorded in CeM neurons before and after CNO application. Scale bars, 20 pA and 25 ms. Right, BLA-evoked EPSC Pr before and after CNO application (time 0; $n = 8$). (**h**) BLA-evoked EPSC Pr before and after CNO application in control conditions ($n = 8$; $P = 0.02$) and in the presence of CPT ($n = 7$; $P = 0.3$) and AM251 ($n = 6$; $P = 0.02$). We observed a difference in the response to CNO between the control condition and the CPT condition (two-way ANOVA indicated a significant effect of CNO ($P < 0.001$) and interaction with the experimental condition ($P < 0.001$); *post hoc* Holm–Sidak-corrected for two comparisons ($P < 0.001$)) but not between control and AM251 conditions ($P = 0.1$). $^{*}P < 0.05$, $^{**}P < 0.01$; Student's paired *t*-test. $^{\#\#\#}P < 0.001$; two-way ANOVA, *post hoc* Holm–Sidak; n.s., nonsignificant ($P > 0.05$). Data in **d–h** are mean ± s.e.m.

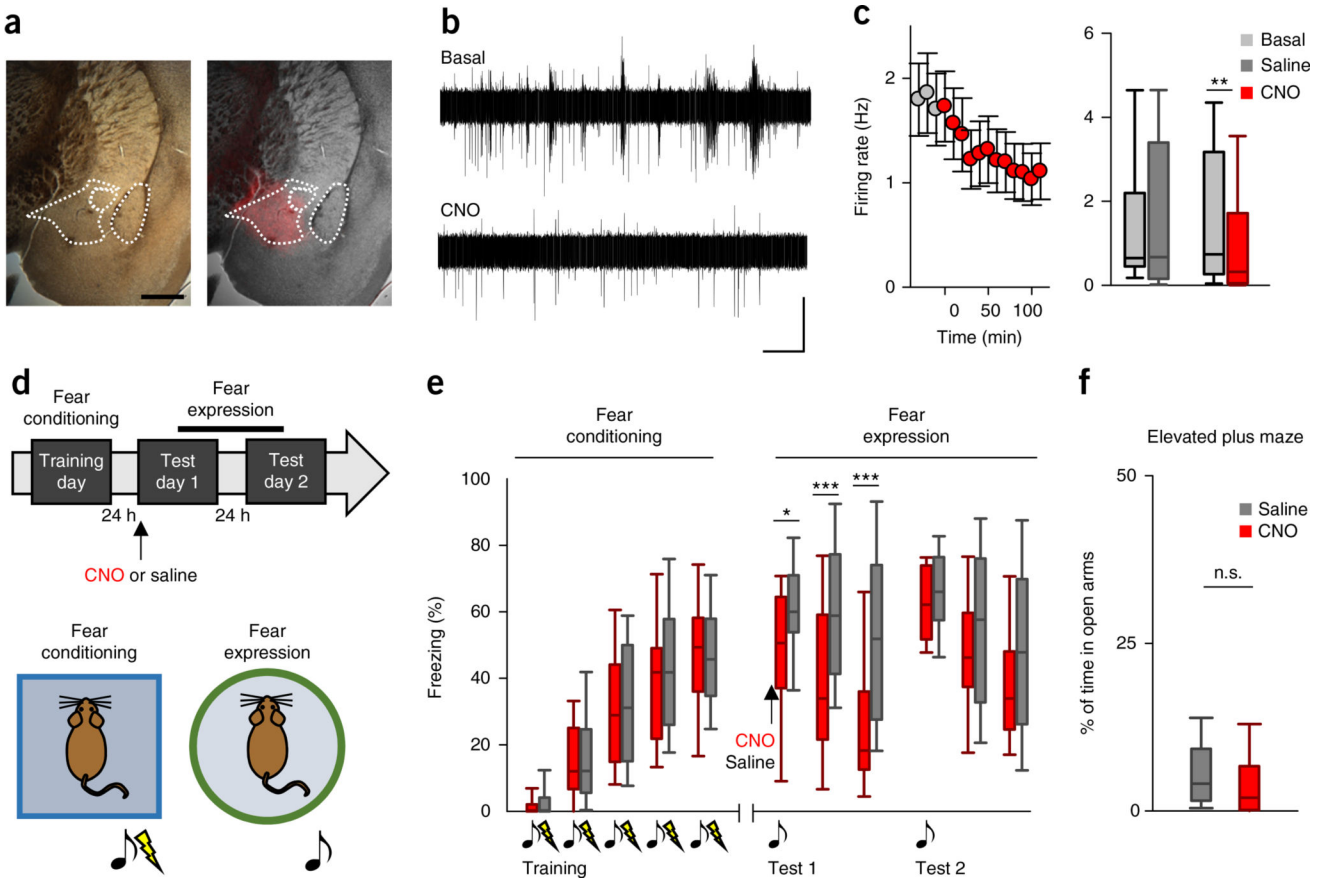

Figure 4.

Selective activation of astrocytic DREADDs in CeM reduces the firing rate and decreases fear expression in a delayed fear conditioning paradigm. (**a**) Images showing DREADD expression in the CeM. Scale bar, 500 μm. (**b**) Representative multi-unit activity recordings in the CeM before and after CNO i.p. injection. Scale bars, 50 μV and 60 s. (**c**) Left, the mean CeM firing rate before (gray) and after CNO application (red; application at time 0). Data shown are mean ± s.e.m. (red; application at time 0, $n = 28$). Right, the CeM firing rate in basal conditions and after saline application ($n = 23$; $P = 0.6$) or CNO application ($n = 28$; $P = 0.004$). (**d**) A schematic representing the delayed fear conditioning paradigm. Mice were fear conditioned on the training day in five trials consisting of a 15-s sound cue co-terminating with a 1-s foot shock. Fear retrieval was measured on test days 1 and 2, with either CNO or saline injected intraperitoneally 30 min before the first cue presentation only in test 1. (**e**) Left, fear response measured as the percentage of freezing during the 15-s cue presentation in CeM DREADD-expressing mice during fear conditioning. Right, fear response measured as the percentage of freezing during the 3 min of continuous cue presentation; data are depicted in 1-min time bins. One nonreinforced cue was presented in test 1 ($P = 0.037$, $P < 0.001$, $P < 0.001$) and in test 2 ($P = 0.23$, $P = 0.24$, $P = 0.066$; $n = 33$ mice injected with CNO (red) and 30 mice injected with saline (gray)). (**f**) The percentage of time spent in the open arms in the elevated plus maze test ($n = 30$ mice injected with CNO and 33 mice injected with saline). *$P < 0.05$, **$P < 0.01$, ***$P < 0.001$; Student's paired t-test (**b**) or unpaired t-test (**e,f**). In box-and-whisker plots, center lines indicate medians, box

edges represent the interquartile range, and whiskers extend to the 10th and 90th percentiles of the distribution.